Polarization Independent Ultra-wideband Meta-material Absorber Using Conductive Ink Resonator

Bharti Kumari, Abhinav Kumar, Prashant Kumar, and Mintu Singh

Bhagalpur College of Engineering, Bhagalpur, Bihar, India

https://doi.org/10.26636/jtit.2024.1.1392

Abstract — A wideband meta-material absorber with square and circular split rings that is based on a frequency selective surface of conductive ink is proposed. With over 90% absorptivity, the structure demonstrates broad absorption for the C, X, KU, and K bands, as well as polarization independent characteristics for both TE and TM, at angles of up to 45°. Research has been performed to better understand the absorption phenomenon by looking into real and imaginary permittivity, permeability, normalized impedance, and surface current density. The meta-material absorber (MA) discussed in this study finds use in defense-related applications, such as radar surveillance, stealth technology, terrestrial and satellite communications.

Keywords — meta-material absorber, microwave absorber, wide-band absorber

1. Introduction

Meta-materials are artificially designed substances capable of achieving specific properties to control electromagnetic wave radiation. This helps absorb or reflect EM waves from the surface. They are characterized by a periodic arrangement of atoms, negative permittivity, negative permeability, and a negative refractive index. Meta-materials can be used for a variety of purposes, including antennas [1], cloaking [2], perfect lenses [3], sensors [4] and absorbers [5]. Meta-material absorbers (MAs) are in the focus of this study due to their absorption-related properties, easy fabrication, as well as the fact that they are ultrathin and light weight. Some of the applications of MAs include stealth technology, EM compatibility, and anechoic chamber design.

A meta-material absorber is a three-layered substance that is designed to absorb incident electromagnetic waves. The middle layer has a dielectric substrate that is excited by a magnetic field generated by current flowing through the upper and lower layers in opposing directions. The top layer, meanwhile, consists of a resonator that is electrically excited at the resonance frequency. The incident power signal cannot pass through the bottom layer, since it is composed of copper. Permittivity and permeability values are adjusted by means of altering electric resonance and magnetic resonance values to bring the structure's input impedance in line with free space impedance. If electric and magnetic excitation occurs simultaneously, the maximum level of absorption is achieved.

First, a single band MA was proposed by Land [6], and this concept attracted the attention of numerous researchers focusing on designing meta-material absorbers. Many different meta-material absorbers, such as those of single-band [7], dual-band [8] or wideband [9] variety, have been introduced. Nowadays, wideband absorbers absorb incident EM waves within a broad frequency range. Different resonant structures are combined to enhance the bandwidth of wideband absorbers. However, such an approach results in considerable dimensions of the unit cell structure [10]. Another approach relies on the multilayer design, where layers of different dimensions are stacked together, increasing the thickness of the structure and restricting the applicability of this particular type [11]. Bandwidth can also be expanded by using a chip resistor, but in this case, the fabrication process becomes more complex [12].

This work proposes a wideband meta-material absorber with square and circular splits rings and a conductive ink frequency-selective surface. The bandwidth of the absorber is 15.84 GHz from 6.28 GHz to 22.10 GHz with more than 90% absorptivity. The proposed MA is examined for both polarizations and various angles of incidence, under normal and oblique incidents.

2. Unit Cell Geometry

In a perfect MA material, absorptivity should be approximately equal to one. Such a parameter can be determined by [13]:

$$A(\omega) = 1 - |S_{11}|^2 - |S_{21}|^2 \,, \tag{1}$$

where S_{11} is the reflection coefficient and S_{21} is the transmission coefficient.

Since the bottom layer is made of copper, there no RF energy is transmitted. Therefore, $|S_{21}|^2 \rightarrow 0$ and thus absorption fully depends on $|S_{11}|^2$. For better absorption, S_{11} should be low, and that can be achieved by impedance matching.

Figure 1 shows the structure of the proposed absorber, with four layers. The top layer is made up of ink, with its bulk conductivity equaling 664 S/m. It consists of a square split ring and two circular rings. Its dimensions are $a = 16$, $b = 14$, $g = 1$, $w_1 = 0.5$, $w_2 = 0.6$, $w_3 = 0.4$, $r_1 = 3$, $r_2 = 5$, $t_{air} = 4$, $t_c = 0.017$, $t_{ink} = 0.1$ [mm]. The next

This work is licensed under a Creative Commons Attribution 4.0 International (CC BY 4.0) License.
For more information, see https://creativecommons.org/licenses/by/4.0/

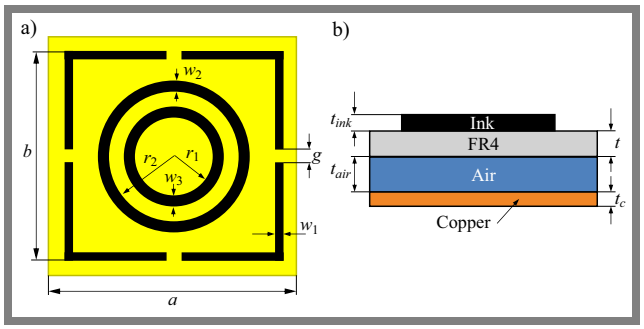

Fig. 1. Top view (a) and side view (b) of a unit cell.

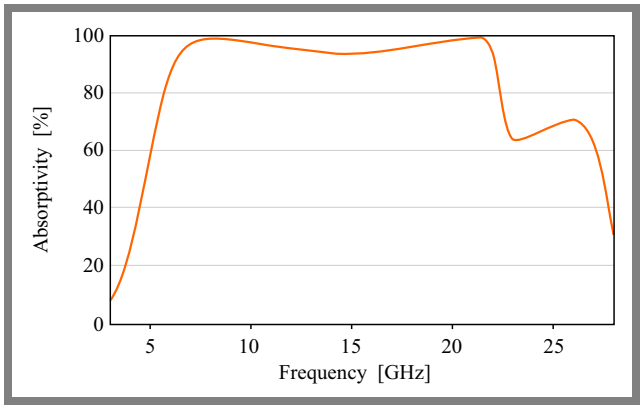

Fig. 2. Simulation of absorptivity for the proposed absorber.

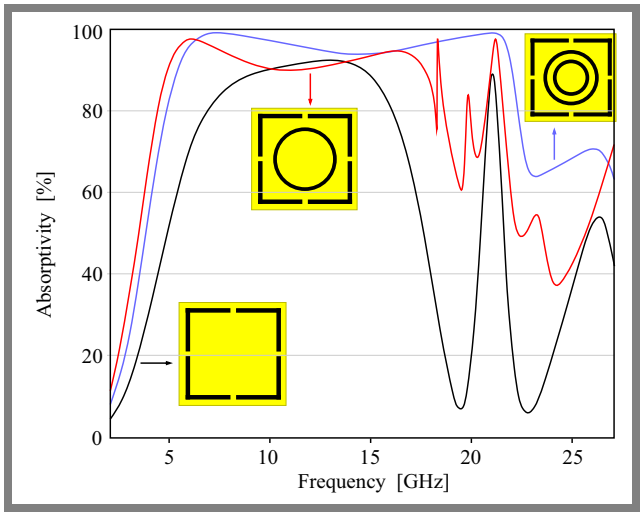

Fig. 3. Absorptivity response for different parts of the resonance structure.

layer is composed of a dielectric substrate (FR4) of thickness $0.0142\,\lambda_0$, dielectric permittivity of $\varepsilon_r = 4.4$ and loss tangent $\delta = 0.02$. The air gap between the bottom layer and the dielectric is 4 mm. The bottom layer is made of copper. The proposed structure provides bandwidth of 15.84 GHz with more than 90% absorptivity from 6.28 GHz to 22.12 GHz, as depicted in Fig. 2.

3. Design Process

In order to assess the impact of absorption response spectra on different parts of the resonance structure, several simulation scenarios have been examined, as shown in Fig. 3. Each resonance structure is responsible for absorption and a selected bandwidth. The rectangular split ring is responsible for two resonances i.e. at 21.18 GHz with more than 85% absorptivity, while absorptivity of over 90% is observed for a range from 10.39 GHz to 15.14 GHz. The placement of a circular ring inside the rectangular split ring results in 90% of absorptivity within the 5.64 GHz to 18.16 GHz bandwidth. To achieve an even greater absorption bandwidth, another ring is placed inside the outer circular ring. Such a structure exhibits wideband absorption in the 15.84 GHz range, i.e. from 6.28 GHz to 22.12 GHz, with absorptivity exceeding 90%.

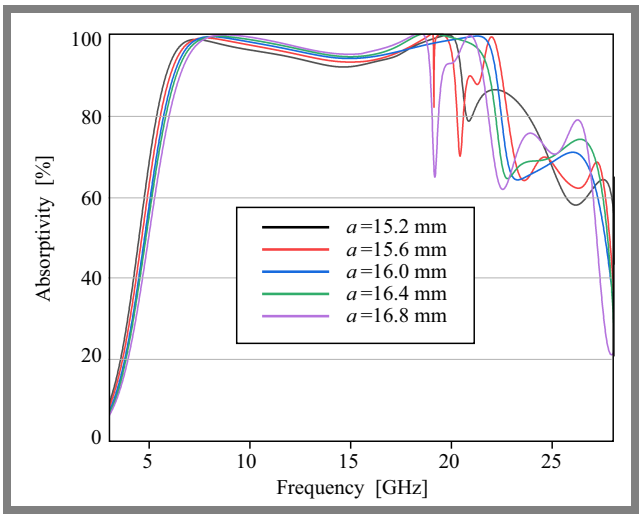

Fig. 4. Simulated absorptivity under varying unit cell lengths.

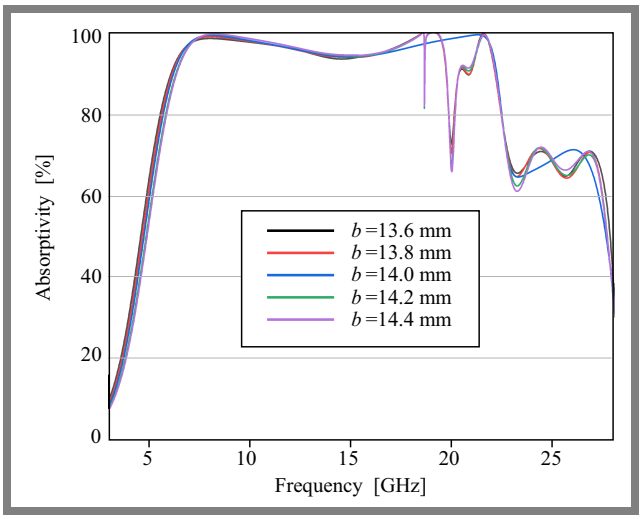

Fig. 5. Simulated absorptivity versus square resonator length.

4. Design Analysis

To verify the design concept and assess the MA parameters, the proposed structure is simulated using Ansys HFSS 15.0 software with periodic boundaries conditions and Floquet port excitation. Figure 4 shows the performance of the designed structure after varying the length of unit cell a to verify absorptivity. It can be observed that the highest bandwidth

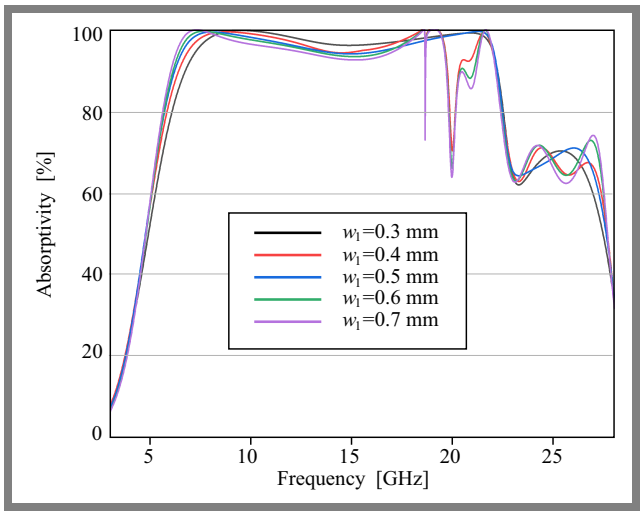

Fig. 6. Simulated absorptivity under different square resonator width values.

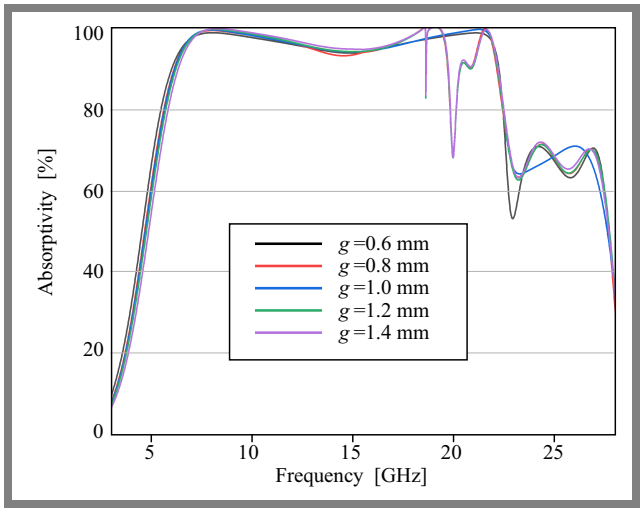

Fig. 7. Simulated absorptivity while varying the square resonator's split.

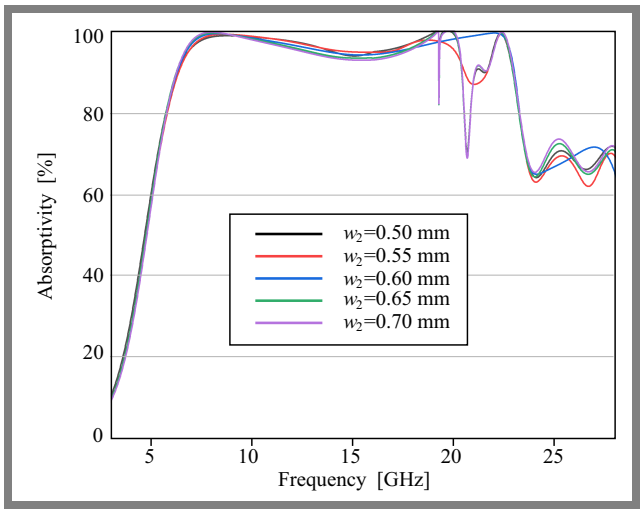

Fig. 8. Simulated absorptivity under varying outer circular ring widths.

(15.84 GHz) is achieved at $a = 16$ mm. In the subsequent analysis, the length of the square resonator b is varied from

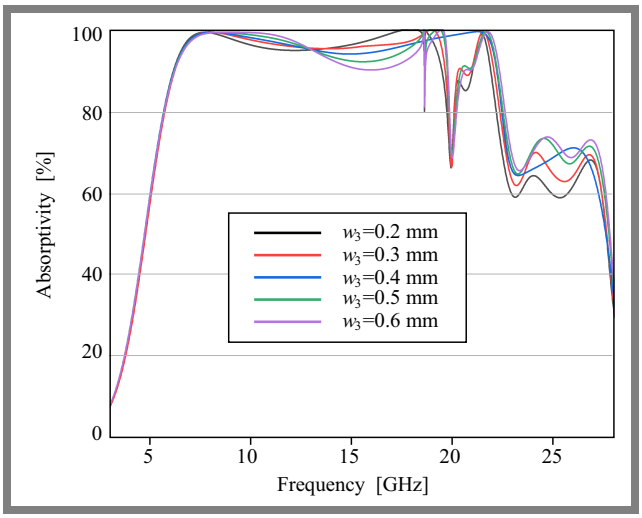

Fig. 9. Simulated absorptivity under different inner circular ring width values.

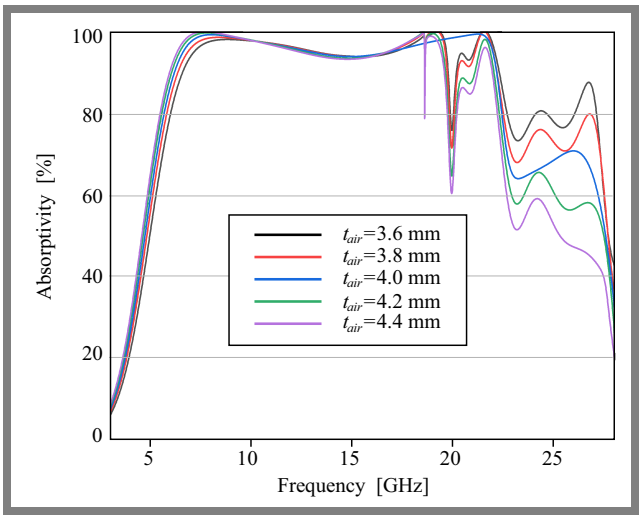

Fig. 10. Simulated absorptivity versus air layer thickness.

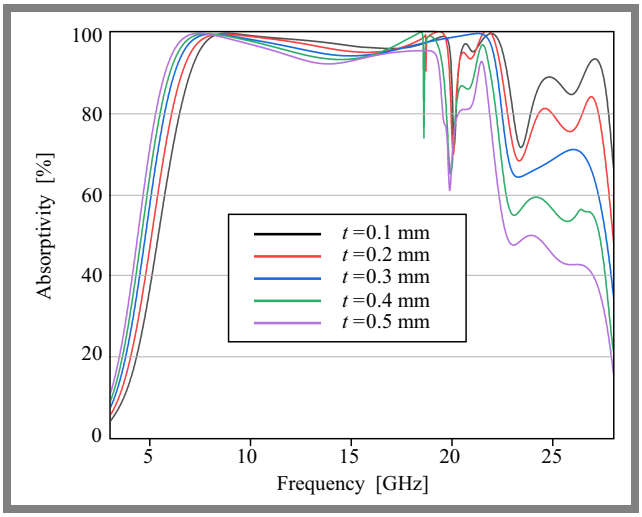

Fig. 11. Simulated absorptivity under varying substrate thickness values.

13.6 to 14.4 mm, with a 0.2 mm step. Figure 5 shows the absorption rate, with the maximum bandwidth at $b = 14$ mm.

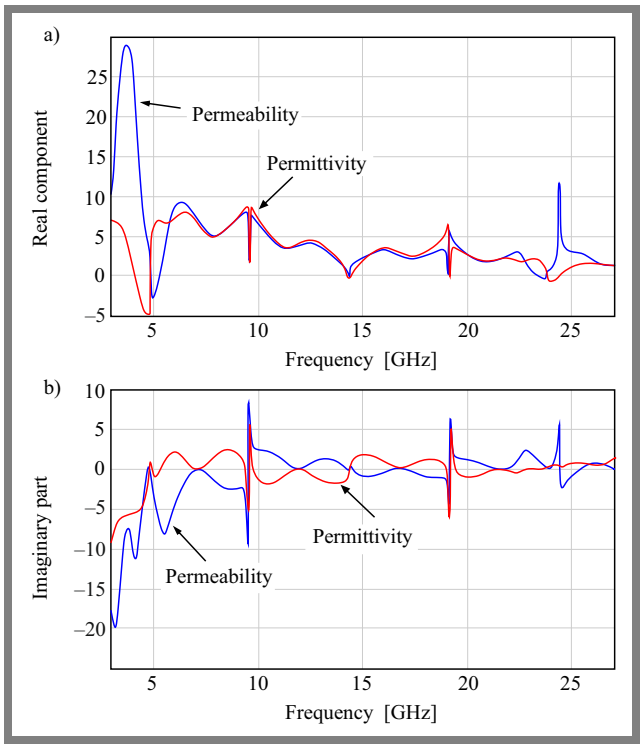

Fig. 12. Real component of ε_{eff} and μ_{eff} of the proposed absorber a) and imaginary part of ε_{eff} and μ_{eff} b).

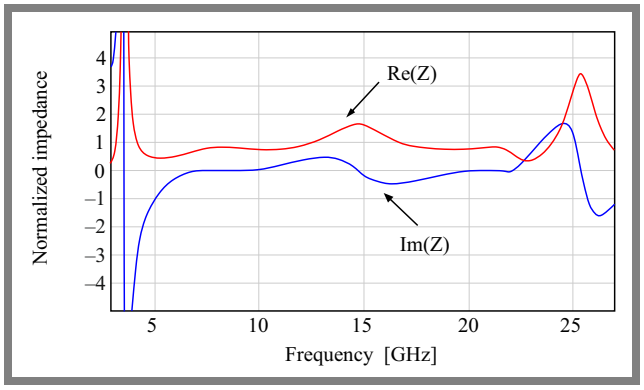

Fig. 13. Normalized impedance of the proposed absorber.

The absorption response of the proposed structure is shown in Fig. 6, where the width of the square resonator w_1 is varied within the 0.3 to 0.7 mm range. It is evident that at $w_1 = 0.5$ mm, the maximum absorption bandwidth is found.
The absorptivity response of the square resonator's split g is presented in Fig. 7, where the width is adjusted between 0.6 and 1.4 mm. The maximum bandwidth is reached at $g = 1$ mm.
Figure 8 displays the absorptivity of the outer circular ring, with its width varying from $w_2 = 0.5$ to 0.7 mm. It can be noticed that a wide bandwidth is obtained at $w_2 = 0.6$ mm.
The width of the inner circular ring w_3 varies from 0.2 to 0.6 mm, and the related absorptivity response is shown in Fig. 9. It can be noticed that the optimal bandwidth is obtained at $w_3 = 0.4$ mm.
In the next step, thickness of air layer is varied from $t_{air} = 3.6$ mm to $t_{air} = 4.4$ mm, and the corresponding absorptivity

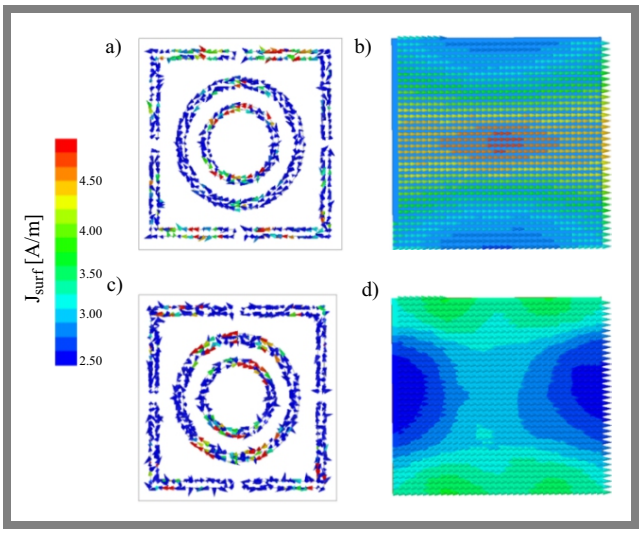

Fig. 14. Surface current distribution on: a) top layer at 8.04 GHz, b) bottom layer at 8.04 GHz, c) top layer at 21.21 GHz, and d) bottom layer at 21.21 GHz.

response is shown in Fig. 10. The figure confirms that the maximum bandwidth can be achieved at $t_{air} = 4$ mm.
In the last test, the absorption response of the proposed structure is measures for varying substrate thickness values (from $t = 0.1$ to $t = 0.5$ mm). It can be observed that the optimal bandwidth is achieved at $t = 0.3$ mm (Fig. 11).

5. Absorption Mechanism

The absorption characteristics of MA follow Eq. (1) and depend on S_{11} and S_{21} parameters. Because of the copper layer used on the bottom, the transmission coefficient drops to zero, which reduces the reflectivity from the absorber's structure and increases absorptivity. Equation (2) provides an alternative expression for the reflection coefficient that is based on the medium's effective impedance [14].

$$S_{11} = \frac{Z_{eff} - Z_0}{Z_{eff} + Z_0} \,. \tag{2}$$

When the free space impedance and the structure's impedance Z_{eff} are equal, S_{11} achieve the minimum value. Impedance of the structure may be written in the form of permittivity and permeability of the absorber, by Eq. (3) [15].

$$Z_{eff} = \sqrt{\frac{\mu_o\,\mu_{eff}}{\varepsilon_0\,\varepsilon_{eff}}} = Z_0\sqrt{\frac{\mu_{eff}}{\varepsilon_{eff}}} = Z_0\sqrt{\frac{\mu + j\mu'}{\varepsilon + j\varepsilon'}} \,. \tag{3}$$

Free space impedance and normalized impedance are given as [15]:

$$Z_0 = \sqrt{\frac{\mu_0}{\varepsilon_0}} = 377\ \Omega \,, \tag{4}$$

$$Z = \frac{Z_{eff}}{Z_0} \,. \tag{5}$$

As shown in Fig. 13, the real part of normalized input impedance of the proposed absorber changes to unity and imaginary part becomes zero from the 6.28 GHz to 22.10 GHz frequency regime. The real part of permittivity and permeability is equal and their imaginary part becomes zero in the design frequency regime, which leads to impedance

matching depicted in Fig. 12. This proves that the MA and free space are ideally impedance-matched, resulting in maximum absorption.

In order to investigate the absorption mechanism, current distributions of the proposed wideband absorber's top and bottom surfaces are examined at two absorption peak frequencies, as illustrated in Fig. 14. At 8.04 GHz, the surface current is mainly localized in the inner and the outer circular ring, and also in some parts of the rectangular ring, whereas absorption at high frequency stems mostly from the surface current in the inner circular ring and rectangular ring. The surface current flows present in the top and bottom layers oppose each other, as shown in Fig. 14, which creates magnetic resonance and adjusts the permeability of the structure so that its impedance is equal to that of free space.

At these resonating frequencies, the patch array is electrically excited by an incident electric field. The magnetic field and the strong electric field can be observed to create a significant amount of absorption in the same area, at this specific frequency. Therefore, the absorption peak at that frequency is affected by the combined effects of both E and H fields.

6. Polarization Insensitive Behavior

Here, both normal and oblique incidence is examined for the proposed MA. The normal and oblique wave incidence of the proposed structure is examined. It is polarization insensitive due to the symmetric MA structure. In the case of normal incidence, electric and magnetic field directions rotate at various angles, i.e., polarization angle φ, while the wave propagation direction is normal along the z axis. The polarization angle is changed from 0 to 90° at 15° increments. As shown in Fig. 15, it is evident that absorptivity remains constant.

Under oblique incidence, both TE and TM modes are examined for the proposed structure. The incidence angle θ is varied while φ remains constant to assess absorptivity changes. The electric field in TE polarization is constant and perpendicular to the plane of incidence, but the magnetic field and wave propagation direction have been rotated at different angles varying from 0 to 45°. In TM polarization, the electric field and wave propagation direction have been rotated from 0 to 45°, whereas the magnetic field is constant and perpendicular to the plane of incidence.

The absorptivity curve shown in Fig. 16 decreases along with an increasing angle incidence. The proposed structure exhibits high absorptivity (exceeding 80%) up to an incidence angle of 45°.

7. Conclusion

A polarization-independent wideband meta-material absorber based on conductive ink with a frequency selective surface has been discussed. The absorber offers an innovative feature, namely broad-spectrum absorption achieved thanks to more than 90% absorptivity, covering a frequency range of 6.28 to 22.12 GHz. Surface current density and input impedance were analyzed as well to understand the absorption mechanism. Both normal and oblique angles of incidence were examined in relation to the structure's polarization behavior. The proposed structure is characterized by polarization insensitivity. For both TE and TM polarizations, it offers an absorption rate of over 80%, with an oblique incidence angle of up to 45°. It is ultrathin, which makes it suitable for satellite communications as well as stealth and radar applications.

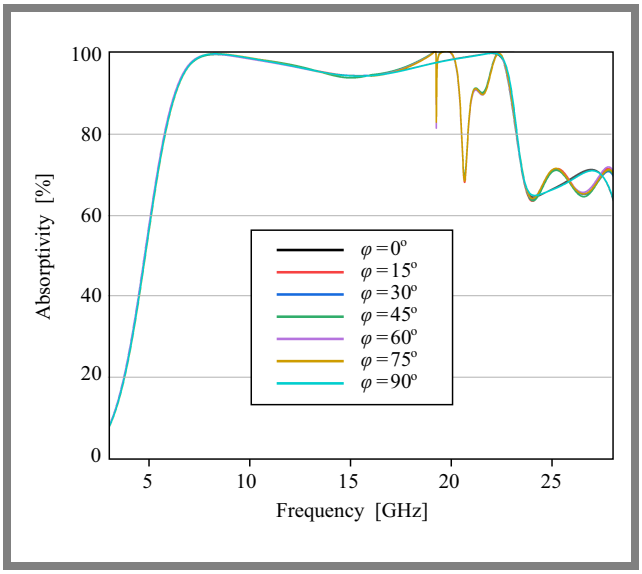

Fig. 15. Simulated absorptivity versus polarization angles.

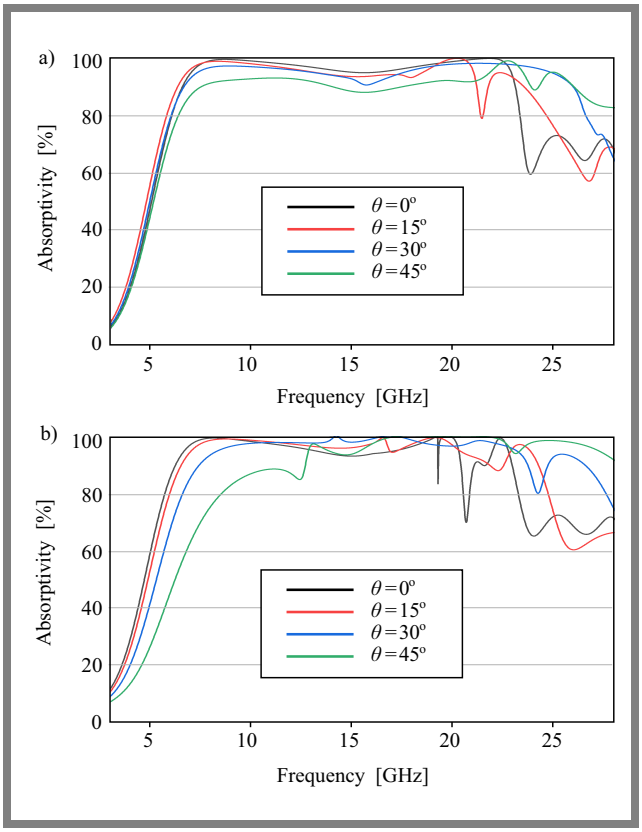

Fig. 16. Simulated absorptivity at different incidence angles under: a) TE and b) TM polarization.

Tab. 1. Comparison of the proposed MA with other works.

Reference	Cell size $[\lambda_0 \times \lambda_0]$	Shape	Material	Absorption bandwidth	Thickness $[\lambda_0]$	Normal incidence	Oblique angle incidence	
							TE	TM
[16]	0.39 × 0.39	Square	FR4, copper	12.80–16.64 GHz (90%)	0.049	Polarization sensitive	$A(\omega) > 70\%$ up to 60°	N/A
[17]	0.16 × 0.16	Square	FR4, copper	3.90–10 GHz (90%)	0.098	Polarization independent	$A(\omega) > 50\%$ up to 75°	$A(\omega) > 50\%$ up to 75°
[15]	0.35 × 0.35	Square	FR4, copper	14.44–27.87 GHz	0.1134	Polarization sensitive	$A(\omega) > 80\%$ up to 45°	$A(\omega) > 80\%$ up to 45°
[18]	0.26 × 0.26	Square	FR4, copper	1.92–2.26 GHz (80%)	0.022	Polarization independent	$A(\omega) > 70\%$ up to 45°	$A(\omega) > 70\%$ up to 45°
[19]	0.023 × 0.023	Square	VO2, gold, polyimide	3.5–8 THz (90%)	0.013	Polarization independent	$A(\omega) > 80\%$ up to 60°	$A(\omega) > 70\%$ up to 60°
[20]	0.34 × 0.34	Square	FR4, copper	5.94–16.84 GHz (80%)	0.120	Polarization sensitive	$A(\omega) > 80\%$ up to 45°	$A(\omega) > 80\%$ up to 45°
Proposed	0.75 × 0.75	Square	FR4, copper, ink	6.28–22.1 GHz (90%)	0.0142	Polarization independent	$A(\omega) > 80\%$ up to 45°	$A(\omega) > 80\%$ up to 45°

References

[1] C. Barde, A. Choubey, R. Sinha, S.K. Mahto, and P. Ranjan, "A Novel ZOR-inspired Patch Antenna for Vehicle Mounting Application", *Ambient Communications and Computer Systems*, pp. 47–53, 2019 (https://doi.org/10.1007/978-981-13-5934-7_5).

[2] D. Schurig *et al.*, "Metamaterial Electromagnetic Cloak at Microwave Frequencies", *Science*, vol. 314, no. 5801, pp. 977–980, 2006 (https://doi.org/10.1126/science.1133628).

[3] N. Fang and X. Zhang, "Imaging Properties of a Metamaterial Superlens", in: *Proc. of the 2nd IEEE Conference on Nanotechnology*, Washington, USA, 2002 (https://doi.org/10.1109/NANO.2002.1032233).

[4] R. Yahiaoui *et al.*, "Multispectral Terahertz Sensing with Highly Flexible Ultrathin Metamaterial Absorber", *Journal of Applied Physics*, vol. 118, no. 8, 2015 (https://doi.org/10.1063/1.4929449).

[5] P. Ranjan, A. Choubey, S. Kumar, and R. Sinha, "An Ultrathin Five-band Polarization Insensitive Metamaterial Absorber Having Hexagonal Array of 2D-bravais-lattice", *Progress in Electromagnetics Research C*, vol. 87, pp. 13–23, 2018 (https://doi.org/10.2528/PIERC18061907).

[6] N.I. Landy, S. Sajuyigbe, J.J. Mock, and D.R. Smith, "Perfect Metamaterial Absorber", *Physical Review Letters*, vol. 100, no. 20, art. no. 207402, 2008 (https://doi.org/10.1103/PhysRevLett.100.207402).

[7] Z. Yin, Y. Lu, S. Gao, and J. Yang, "Optically Transparent and Single-band Metamaterial Absorber Based on Indium-tin-oxide", *International Journal of RF and Microwave Computer-Aided Engineering*, vol. 29, no. 4, art. no. 21536, 2019 (https://doi.org/10.1002/mmce.21536).

[8] M. Li, Y. Helin, X.-W. Hou, and Y. Tian, "Perfect Metamaterial Absorber with Dual Bands", *Progress in Electromagnetics Research*, vol. 108, pp. 37–49, 2010 (https://doi.org/10.2528/PIER10071409).

[9] L. Liu, Y. Zang, H. Zhai, and C. Zhan, "Reconfigurable Wideband Metamaterial Absorber with Wide Angle and Polarisation Stability", *Electronics Letters*, vol. 51, no. 21, pp. 1624–1626, 2015 (https://doi.org/10.1049/el.2015.1557).

[10] S. Li *et al.*, "Wideband, Thin, and Polarization-insensitive Perfect Absorber Based the Double Octagonal Rings Metamaterials and Lumped Resistances", *Journal of Applied Physics*, vol. 116, no. 4, 2014 (https://doi.org/10.1063/1.4891716).

[11] Y. Liu, X. Hao, and S. An, "Significant Enhancement of Energy-storage Performance of (Pb0. 91La0. 09)(Zr0. 65Ti0. 35) O3 Relaxor Ferroelectric Thin Films by Mn Doping", *Journal of Applied Physics*, vol. 114, no. 17, 2013 (https://doi.org/10.1063/1.4829029).

[12] F. Ding, Y. Cui, X. Ge, Y. Jin, and S. He, "Ultra-broadband Microwave Metamaterial Absorber", *Applied Physics Letters*, vol. 100, no. 10, 2012 (https://doi.org/10.1063/1.3692178).

[13] O. Ayop *et al.*, "Triple Band Circular Ring-shaped Metamaterial Absorber for X-band Applications", *Progress in Electromagnetics Research M*, vol. 39, pp. 65–75, 2014 (https://doi.org/10.2528/PIERM14052402).

[14] Md. Moniruzzaman *et al.*, "Quad Band Metamaterial Absorber Based on Asymmetric Circular Split Ring Resonator for Multiband Microwave Applications", *Results in Physics*, vol. 19, art. no. 103467, 2020 (https://doi.org/10.1016/j.rinp.2020.103467).

[15] C. Barde, A. Choubey, and R. Sinha, "Wide Band Metamaterial Absorber for Ku and K Band Applications", *Journal of Applied Physics*, vol. 126, no. 17, 2019 (https://doi.org/10.1063/1.5119311).

[16] R. Sekar and S.R. Inabathini, "An Ultra-thin Compact Wideband Metamaterial Absorber", *Radioengineering*, vol. 27, no. 2, pp. 364–372, 2018 (https://doi.org/10.13164/re.2018.0364).

[17] S. Kalraiya, R.K. Chaudhary, and M.A. Abdalla. "Design and Analysis of Polarization Independent Conformal Wideband Metamaterial Absorber Using Resistor Loaded Sector Shaped Resonators", *Journal of Applied Physics*, vol. 125, no. 13, 2019 (https://doi.org/10.1063/1.5085253).

[18] K.P. Kaur, T. Upadhyaya, and M. Palandoken, "Ultrathin Wideband Polarization Independent Compact Metamaterial Microwave Absorber", in: *2018 28th International Conference Radioelektronika*, Prague,

Czech Republic, 2018 (https://doi.org/10.1109/RADIOELEK.2018.8376395).

[19] L. Wang, D. Xia, Q. Fu, X. Ding, and Y. Wang, "A Switchable Ultra-Wideband Metamaterial Absorber with Polarization-insensitivity and Wide-incident Angle at THz Band", *Frontiers in Materials*, vol. 8, art. no. 729495, 2021 (https://doi.org/10.3389/fmats.2021.729495).

[20] S. Bhattacharyya, S. Ghosh, and K.V. Srivastva, "A Microwave Meta-material Absorber with Wide Bandwidth", in: *2016 URSI Asia-Pacific Radio Science Conference (URSI AP-RASC)*, Seoul, South Korea, 2016 (https://doi.org/10.1109/URSIAP-RASC.2016.7601147).

Bharti Kumari, B.Tech.
Department of Electronics and Communication Engineering
https://orcid.org/0009-0003-1210-4421
E-mail: goldi02032001@gmail.com
Bhagalpur College of Engineering, Bhagalpur, Bihar, India
https://www.bcebhagalpur.ac.in

Abhinav Kumar, M.Tech.
Department of Electronics and Communication Engineering
https://orcid.org/0009-0000-0331-1929
E-mail: abhinavbceece@gmail.com
Bhagalpur College of Engineering, Bhagalpur, Bihar, India
https://www.bcebhagalpur.ac.in

Prashant Kumar, Ph.D., Assistant Professor
Department of Electronics and Communication Engineering
http://orcid.org/0000-0002-5296-7366
E-mail: pkumar.mnnit@gmail.com
Bhagalpur College of Engineering, Bhagalpur, Bihar, India
https://www.bcebhagalpur.ac.in

Mintu Singh, M.Tech.
Computer Science & Engineering
http://orcid.org/0009-0000-5220-0301
E-mail: mintucemk.singh@gmail.com
Bhagalpur College of Engineering, Bhagalpur, Bihar, India
https://www.bcebhagalpur.ac.in